Intergranular trace elements in mantle xenoliths from Russian Far East: Example for mantle metasomatism by hydrous melt

Island Arc (2009) **18**, 225–241

Research Article

Intergranular trace elements in mantle xenoliths from Russian Far East: Example for mantle metasomatism by hydrous melt

JUNJI YAMAMOTO,[1,2]* SHUN'ICHI NAKAI,[3] KOSHI NISHIMURA,[2] ICHIRO KANEOKA,[3] HIROYUKI KAGI,[4] KEIKO SATO,[5] TASUKU OKUMURA,[6] VLADIMIR S. PRIKHOD'KO[7] AND SHOJI ARAI[8]

[1]*Woods Hole Oceanographic Institution, Woods Hole, MA 02543, USA (email: jyamamoto@whoi.edu),* [2]*Institute for Geothermal Sciences, Kyoto University, Noguchibaru, Beppu, Oita 874-0903,* [3]*Earthquake Research Institute, University of Tokyo, 1-1-1 Yayoi, Bunkyo-ku, Tokyo 113-0032,* [4]*Geochemical Laboratory, University of Tokyo, 7-3-1 Hongo, Bunkyo-ku, Tokyo 113-0033,* [5]*IFREE, Japan Agency for Marine-Earth Science and Technology, 2-15 Natsushima, Yokosuka 237-0061,* [6]*Research Institute of Natural Sciences, Okayama University of Science, 1-1 Ridai-cho, Okayama 700-0005,* [7]*Institute of Tectonics and Geophysics (Far Eastern Branch, Russian Academy of Sciences), 65 Kim Yu Chen Str., Khabarovsk 680063, Russian Federation, and* [8]*Department of Earth Sciences, Faculty of Science, Kanazawa University, Kakuma, Kanazawa 920-1192, Japan*

Abstract Based on both major and trace element chemistry, the occurrence of the intergranular component in mantle-derived xenoliths from far eastern Russia has been constrained. Whole-rock trace element measurements of one xenolith show apparent negative anomalies in Ce, Th, and high field strength elements on normalized trace element patterns. The trace element pattern of the whole rock differs from those of constituent minerals, indicating that the anomalies in the whole rock are attributable to the presence of an intergranular component. That assumption was confirmed using *in situ* analysis of trace elements in the intergranular substance and melt inclusion using laser ablation inductively coupled plasma–mass spectrometry. Both the intergranular component and the melt inclusions have identical trace element patterns, which mean that these materials are a cognate metasomatizing agent. The anomalies are regarded as mantle metasomatism related to an aqueous fluid. Hydrous minerals were observed on the wall of the melt inclusions using micro-Raman spectroscopy, indicating that the melt inclusions contained a large amount of water. Thus, this study reveals a trace element composition of a hydrous metasomatizing agent in the mantle.

Key words: intergranular component, LA–ICP–MS, mantle wedge, mantle xenolith, melt inclusion.

INTRODUCTION

Metasomatic changes in mantle rocks would play a key role in determining the chemical and isotopic characteristics of the mantle and mantle-derived magma. In the past 25 years, many studies have been made on the nature of the metasomatizing agents. Coltorti *et al.* (2000) subdivided metasomatizing agents into three types (carbonatite melt, Na-alkaline silicate melt, and K-alkaline silicate melt) based on specific geochemical features which might result from low-degree partial melting at the lithosphere–asthenosphere transition (Dalton & Presnall 1998; Coltorti *et al.* 2000). Adakite melt, which is formed by partial melting of subducted young oceanic crust, is also considered to be a metasomatizing agent (Kepezhinskas *et al.* 1995; Kilian & Stern 2002).

A great deal of effort has been made on identification of the nature of the metasomatizing agents. What seems to be lacking, however, is a metasomatizing agent related to aqueous fluid. For

*Correspondence.

Received 21 December 2007; accepted for publication 2 July 2008.

doi:10.1111/j.1440-1738.2008.00642.x

example, hydrous melts would be formed in the partial melting zone in the mantle wedge. Thus, subduction-related fluid or melt would have a unique trace element composition inherited from aqueous fluid originating in the subducting slab. Recent papers have suggested that trace element compositions of fluid derived from subducted oceanic plate, based on fluid compositions in subducted sedimentary rocks, can be deduced using trace element partition coefficients between zoisite and fluid (Feineman *et al.* 2007) or using a series of high-pressure experiments (Feineman *et al.* 2007; Spandler *et al.* 2007). Large ion lithophile elements (LILE) generally show the highest mobility from the subducted rocks, followed by light rare earth elements (LREE), heavy rare earth elements (HREE), Th, and high field strength elements (HFSE). That inference has been reinforced with observed data that trace element compositions of subducted rocks are strongly dependent upon the prograde P–T path (Bebout *et al.* 2007). A decisive factor in characterizing trace element composition of the hydrous fluid in the mantle wedge is element partitioning during dehydration. That is, the amount of water in a metasomatizing agent may increase the degree of elemental fractionation.

A mantle xenolith from far eastern Russia used in this study has hydrous melt inclusions, whose trace element composition would be fractionated during generation of the melt in the presence of aqueous fluid. Thus, the trace element compositions of the melt offer the key for understanding the nature of hydrous metasomatizing agents. Here we report trace element compositions of whole rock with those of acid-leached major minerals, laser-ablated interstitial components, and melt inclusions of mantle xenoliths from far eastern Russia.

SAMPLES

Extensive tholeiitic and alkaline basaltic volcanism occurred in northeastern China and far eastern Russia in the Cenozoic. The alkaline basalts locally contain abundant upper mantle-derived ultramafic xenoliths (Fig. 1). Environs of sampling points of the xenoliths used in this study are covered with accretionary complexes (Natal'in 1993; Ishiwatari & Tsujimori 2003). The far eastern Russian mantle was therefore a mantle wedge during the Mesozoic to Early Cenozoic. Geodynamic reconstructions take a similar view (Faure & Natal'in 1992; Faure

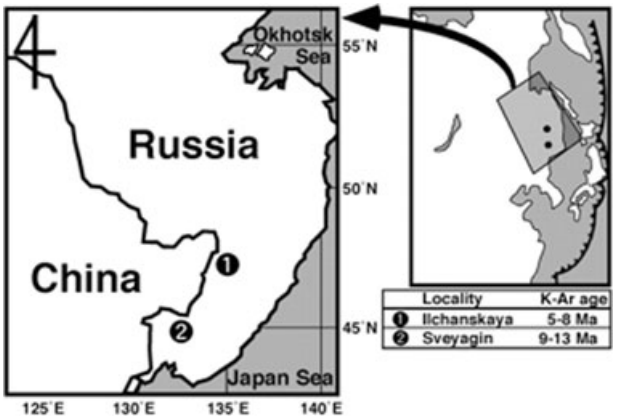

Fig. 1 Sample localities and reference K–Ar ages of the host volcanic bodies. The range of age is estimated from K–Ar dates of alkali basalts around sampling points (Esin & Travin 1994; Sato 2000).

et al. 1995). The basalts erupted long after plate subduction in the far eastern Russia area, which provides considerable advantages for the study of subduction-related fluids in mantle xenoliths. In the case of mantle xenoliths sampled at a presently active convergent margin and island arc, they could be contaminated with present-day subduction-related components from their host magma. Consequently, the mantle xenoliths in this region are suitable for the study of subduction-related subcontinental lithospheric mantle.

The two xenoliths (Ilc-1 and Sv-1) examined in this study are spinel–lherzolites sampled from two localities (Ilchanskaya and Sveyagin) in far eastern Russia (Fig. 1). They are sufficiently large for several major and trace element analyses. Samples Ilc-1 and Sv-1 respectively contain 59.2 and 61.3 vol.% olivine, 28.1 and 22.3 vol.% orthopyroxene, 10.5 and 13.1 vol.% clinopyroxene, and 2.2 and 3.3 vol.% spinel, which were obtained by point-counting. Recent studies have provided some isotopic data related to mantle xenoliths, including both of these xenoliths, on noble gases (Yamamoto *et al.* 2004) and Li–Sr–Nd (Nishio *et al.* 2004). Noble gas isotopic compositions of sample Ilc-1 show no obvious indication of the subduction-related component with radiogenic isotopic compositions (Yamamoto *et al.* 2004), whereas sample Sv-1 shows unusual isotopic compositions of noble gases, Sr, and Nd, which are interpreted as resulting from an infiltration of subduction-related fluid into the mantle wedge (Nishio *et al.* 2004; Yamamoto *et al.* 2004).

The xenoliths were taken from different volcanic bodies with eruption ages of about 5 to 13 Ma (Esin & Travin 1994; Sato 2000 fig. 1). Xenoliths of up to

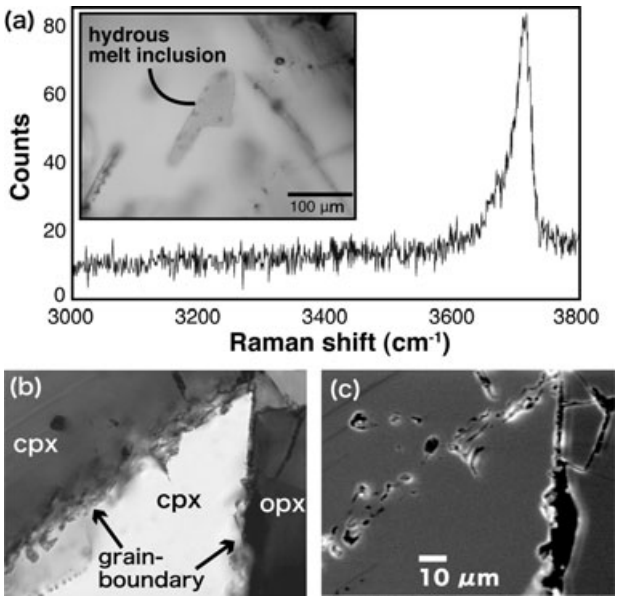

Fig. 2 Photomicrographs of a thin section of a mantle-derived xenolith (Sv-1). (a) melt inclusion in an orthopyroxene and a Raman spectrum of wall of the inclusion (after Yamamoto 2007). Raman band around 3700/cm results from OH stretching mode in a hydrous mineral, (b) intergranular area of xenoliths taken with an open nicol, and (c) backscattered electron image of (b).

several centimeters in width are commonly observed in the region, but some are larger, about 20 cm. They consist of olivine, orthopyroxene, and clinopyroxene, with lesser amounts of chromian spinel, and show protogranular textures. The average diameters of these mineral particles for samples Ilc-1 and Sv-1 are, respectively, about 1.5 and 0.5 mm. All constituent minerals of samples Ilc-1 and Sv-1 have melt inclusions. Trails of the melt inclusions occasionally crosscut grain boundaries. In sample Sv-1, hydrous minerals were frequently observed on the wall of the melt inclusions using micro-Raman spectroscopy, indicating that they were hydrous melts in the mantle (Fig. 2a). Although a substance is visible in the intergranular area under a microscope, because of its tiny size, we were unable to analyze the major element composition of the intergranular component using electron probe microanalysis (Fig. 2b,c).

METHODS

MAJOR ELEMENT ANALYSES

Major element compositions of the xenoliths constituent minerals were determined using an electron probe microanalyzer (JEOL JXA8800R) at the Earthquake Research Institute, University of Tokyo. Correction procedures followed the method of Bence & Albee (1968) using correction factors by Nakamura & Kushiro (1970). Analyses were carried out using an accelerating voltage of 20 kV and a beam current of 20 nA. Integrated times for measurements were 100 s for most elements and 20 s for Na and K. To detect chemical zonation within individual grains, step-scanning was used. All major element analyses were performed for the core minerals. Five points in each grain and five grains in each xenolith were analyzed. Table 1 shows the average compositions of 25 measurements for each mineral species.

TRACE ELEMENT ANALYSES

At the Earthquake Research Institute, University of Tokyo, trace elements in minerals decomposed by an acid treatment were analyzed for olivine, orthopyroxene, clinopyroxene, and whole rocks for two xenoliths (Ilc-1 and Sv-1) using inductively coupled plasma–mass spectrometry (ICP–MS, PQ3, Thermo Elemental). Rocks were cut into approximately 2-mm-thick slabs, which were used as samples representing whole rocks. Trace element contamination during cutting was negligible, as ascertained by scanning analyses using laser ablation ICP–MS (LA–ICP–MS).

Residual rock specimens were roughly crushed; minerals were carefully selected manually. The mineral separates were then washed with 70°C 2 N HNO_3 for 0.5 hour for more complete elimination of the intergranular component. They were then washed ultrasonically in distilled water. The series of treatments reduced the weight by about 2%.

After that treatment, about 100 mg of whole rock or olivine (or 25 and 13 mg for orthopyroxene and clinopyroxene, respectively) of each sample was weighed and finely crushed in an agate mortar filled with distilled water to avoid loss of fragments.

Subsequently, 20 mg of each powdered sample was weighed in a Teflon beaker (or 10 mg for orthopyroxene and clinopyroxene), and 0.3 mL each of 11.5 N $HClO_4$ and 30 N HF was added to the samples. The tightly capped beaker was agitated in an ultrasonic bath for 30 min and heated on a hot plate at 160°C in a draft chamber for 12 h. The decomposed samples were evaporated at 150°C for 3 h and 180°C for 1 h. To decompose the fluoride completely, 0.3 mL of 7 N $HClO_4$ was added and samples agitated in the ultrasonic bath for 15 min at room temperature. This acid treat-

Table 1 Average compositions (wt%) of minerals in ultramafic xenoliths from far eastern Russia

Sample locality	Ilc-1				Sv-1			
rock type	Ilchanskaya lherzolite				Sveyagin lherzolite			
mineral	ol	opx	cpx	sp	ol	opx	cpx	sp
Mg#	89.95	90.30	89.53	77.01	89.81	90.09	90.74	75.78
Cr#				12.23				9.20
SiO_2	40.52	54.16	52.09	0.11	40.14	54.73	52.60	0.02
TiO_2	0.01	0.15	0.48	0.22	0.01	0.12	0.64	0.06
Al_2O_3	0.04	5.57	7.43	55.34	0.00	4.21	7.15	58.93
Cr_2O_3	0.03	0.51	0.91	11.50	0.01	0.19	0.46	8.90
FeO	9.77	6.12	3.31	11.24	9.98	6.56	2.65	11.46
MnO	0.14	0.14	0.10	0.11	0.13	0.14	0.06	0.04
MgO	49.05	31.98	15.89	21.12	49.31	33.44	14.57	20.12
CaO	0.09	1.07	18.08	0.00	0.01	0.47	20.02	0.01
Na_2O	0.01	0.17	1.61	0.01	0.01	0.05	1.73	0.00
K_2O	0.00	0.00	0.01	0.00	0.01	0.01	0.00	0.01
NiO	0.32	0.09	0.05	0.34	0.39	0.08	0.04	0.39
P_2O_5	0.02	0.02	0.05	0.02	0.00	0.00	0.06	0.00
V_2O_3	0.00	0.00	0.00	0.00	0.02	0.02	0.02	0.07
Total	100	100	100	100	100	100	100	100
T [°C]	1097	±16			952	±56		

Multiple points in the core of a single grain of each mineral species were analyzed.
Equilibrium temperatures (T) were estimated by two-pyroxene geothermometer of Wells (1977).
cpx, clinopyroxene; ol, olivine; opx, orthopyroxene; sp, spinel.

ment was duplicated for complete decomposition. During decomposition of whole rocks, spinel remained. We omitted undissolved spinel from analyses because spinel is negligible for the trace element budget of peridotites (Stosch 1982; O'Reilly *et al.* 1991; McDonough *et al.* 1992; Bedini & Bodinier 1999). After drying, 0.75 mL of 7 N HNO_3 was again added and the samples were they agitated in the ultrasonic bath for 15 min. Then they were decomposed at 160°C for 3 h. The decomposed samples were centrifuged for 5 min at 4000 rpm. No sample residue remained after this treatment in any case. One milliliter of the solution was taken out, put in another Teflon beaker, then mixed with 18 mL of 2 wt% HNO_3 containing weak HF. For use in ICP–MS sensitivity calibration, 0.5 mL of 200 ppb indium and rhenium as an internal standard was added to the solution. Then the solution was agitated in the ultrasonic bath for 10 min. Procedural blanks were obtained by strictly following the same procedure as that used for sample measurements. Rock solutions were analyzed without further chemical treatment. Therefore, the precisions of the abundance data are 10% for most elements and 20% for Sr and those with low abundances. Uncertainties in the precision (1σ) include those for sensitivity and blank corrections.

In situ analysis of trace elements was performed using a quadrupole ICP–MS (PQ3, Thermo Elemental) at the Institute for Geothermal Sciences, Kyoto University, equipped with a laser-ablation microprobe (CETAC LSX 500, Cetac Technologies, USA). For the analyses, a UV (266 nm) laser beam was focused onto the surface of a solid sample. The laser used for this study is a Q-switched Nd–YAG laser operated at 7 mJ per pulse. Peak and background regions were selected from the time-resolved spectra of each sample; the selected replicates were averaged to determine the net count rate for each mass. Relative element sensitivities were calibrated against NIST 612 standard glass, with values cross-checked against other well-characterized natural materials including mantle-derived pyroxenes. To quantify the laser yield, ^{44}Ca was used as an internal standard. Replicate analyses of the NIST 610 standard glass indicate an analytical precision of less than 10%.

Materials in melt inclusions or intergranular components were sampled *in situ* using a laser beam. Determination of trace element compositions of the melt inclusion or the intergranular component requires a procedure including signal integration and subtraction of host-mineral contributions. Quantification of the laser yield is possible only for large melt inclusions that have measurable Ca contents. It is difficult to analyze the major element compositions of small melt inclusions (<50 μm) and intergranular components; the surrounding host mineral is usually ablated and mixed with the signal from the intergranular component and the melt inclusion. For the present study, we corrected neither the interelement fractionation

nor host-mineral contributions for LA–ICP–MS analyses of intergranular components and melt inclusions. Nevertheless, trace element patterns for intergranular components and melt inclusions are useful to discern their characteristics because the host mineral has negligible contribution to the patterns.

RESULTS

MAJOR ELEMENT MINERAL CHEMISTRY

Major element contents of constituent minerals of the two mantle xenoliths from far eastern Russia are listed in Table 1. The Fo value ([Mg/(Mg + Fe) × 100] of olivine) and Cr# [Cr/(Cr + Al) × 100] of spinel show uniform values of around 90 and 10, respectively. Those values are typical of upper mantle lherzolite (Arai 1994); their major element compositions suggest that the xenoliths were derived from the fertile upper mantle.

Cores of minerals in the xenoliths are almost homogeneous in terms of major element compositions. The xenoliths probably have a simple cooling history, but the heating episode by host magma is well represented by the reaction coronas surrounding the xenoliths. For example, olivine with a low Fo value and high CaO content is observed only at the margin of the xenoliths. Increased CaO and decrease in Na_2O and Al_2O_3 toward the rim of clinopyroxene are only observed in contact with the host basalt. Therefore, the influence of the host magma is limited to the rim of minerals in the margin of the xenoliths adjacent to the host basalt.

The final equilibrium temperatures before the xenoliths are entrained by the host magma are generally estimated using rim–rim pairs of coexisting minerals. However, we obtained equilibrium temperatures based on core–core pairs of coexisting minerals to avoid chemical disturbances caused by either the host magma or intergranular component. Equilibrium temperatures were estimated based on Wells' (1977) two-pyroxene geothermometer. The equilibrium temperatures are 952 to 1097°C (Table 1), which are within the range of other data of ultramafic xenoliths from far eastern Russia (800 to 1000°C) (Ionov *et al.* 1995) and eastern China (750 to 1100°C) (Fan & Hooper 1989). Geobarometry using micro-Raman spectroscopic analysis of CO_2-dominant inclusions in mantle minerals is promising to elucidate the depth at which the xenoliths were trapped by host magma (Yamamoto *et al.* 2002, 2007; Kawakami *et al.* 2003; Yamamoto & Kagi 2006, 2008). Applying a temperature and pressure condition of a mantle xenolith collected from far eastern Russia (Yamamoto *et al.* 2002), the geothermal gradient around far eastern Russia is estimated to be approximately 26°C/km (Yamamoto & Kagi 2008). Extrapolation of the equilibrium temperatures to intersections with the geothermal gradient indicates that the trapping depths for Ilc-1 and Sv-1 are 43 ± 3 and 35 ± 4 km, respectively, thereby confirming that these xenoliths are of uppermost mantle origin.

TRACE ELEMENTS IN ACID-DECOMPOSED SAMPLES

Abundances of trace elements in acid-leached minerals (olivine, orthopyroxene, clinopyroxene), and whole rock were analyzed for the two samples of Ilc-1 and Sv-1 using ICP–MS (Tables 2,3). Comparison of the trace element patterns for a whole rock and acid-leached constituent minerals of mantle xenoliths are useful to specify the principal host phases for trace elements. Incompatible trace elements tend to occur mostly in clinopyroxene in spinel peridotites (Stosch 1982; Salters & Shimizu 1988; O'Reilly *et al.* 1991; McDonough *et al.* 1992; Bedini & Bodinier 1999). Consequently, the primitive mantle-normalized trace element patterns of clinopyroxene from spinel peridotites usually mimic those of the whole rock as observed in sample Ilc-1 (Fig. 3). The whole rock of sample Ilc-1 shows a nearly flat trace element pattern with slight depletion in HFSE and spikes of highly incompatible elements (Rb and Ba), which is dominated by the pattern of clinopyroxene. In contrast, for the sample Sv-1, the trace element pattern of the whole rock is not correlated with those of the constituent minerals, especially for more incompatible elements (Rb–Sr, Fig. 4). Particularly, the whole-rock pattern shows an LREE-enriched curve in a normalized REE pattern and a clear negative Ce anomaly (Fig. 5). This pattern was confirmed using duplicate analyses. It is noteworthy that the Ce anomaly is not detected in the constituent minerals, except for a slight anomaly observed in orthopyroxene. The pattern of the clinopyroxene of sample Sv-1 shows a slight depletion in LREE, but such a LREE-depleted curve without the Ce anomaly is typical of clinopyroxene from mantle peridotites (Stosch 1982; Bedini & Bodinier 1999). The whole-rock pattern of sample Sv-1 shows clear depletions in Rb, Th, Ce, Sr, and HFSE. We must draw atten-

Table 2 Trace element abundance (ppb) of mineral separates and whole rock of a mantle-derived xenolith (Ilc-1)

Sample	Ilc-1				
mineral	ol	opx	cpx	Whole rock	Whole rock (calculated)
Rb	–	510 ± 80	520 ± 80	1 140 ± 180	202.4 ± 24.5
Pb	–	13.8 ± 0.9	55 ± 4	47 ± 3	9.9 ± 0.5
U	–	5.6 ± 0.3	18.7 ± 1.1	9.2 ± 0.5	3.6 ± 0.1
Th	–	16.9 ± 0.9	30.4 ± 1.6	37 ± 2	8.1 ± 0.3
Ba	125 ± 8.3	2250 ± 70	7 500 ± 200	6 090 ± 190	1 527.4 ± 29.8
Nb	22 ± 1.4	106 ± 12	360 ± 40	360 ± 40	82.1 ± 5.6
Ta	0.91 ± 0.06	6.7 ± 0.3	29.6 ± 1.4	14.1 ± 0.7	5.7 ± 0.2
La	7 ± 0.2	102 ± 4	1 670 ± 60	484 ± 18	213.0 ± 6.5
Ce	14 ± 0.4	226 ± 3	5 500 ± 60	1 043 ± 12	663.7 ± 6.5
Pr	1.49 ± 0.04	31.63 ± 0.15	941 ± 5	166.6 ± 0.8	111.0 ± 0.5
Sr	325 ± 56	3300 ± 400	123 000 ± 15 000	18 000 ± 2 000	14 350.4 ± 1 614.9
Nd	13 ± 0.6	124 ± 3	5 510 ± 140	672 ± 17	635.1 ± 15.1
Hf	1.59 ± 0.08	112 ± 6	1 100 ± 60	117 ± 6	151.3 ± 6.7
Zr	90 ± 7.9	5600 ± 900	40 000 ± 6 000	5 500 ± 900	5 957.7 ± 694.2
Sm	4 ± 0.3	31.7 ± 0.7	1 810 ± 40	251 ± 5	205.6 ± 4.3
Eu	0.40 ± 0.02	23.2 ± 0.8	670 ± 20	79 ± 3	78.9 ± 2.2
Gd	–	72 ± 5	2 460 ± 190	230 ± 18	284.7 ± 20.5
Tb	1.02 ± 0.02	26.4 ± 0.3	443 ± 5	46.9 ± 0.6	55.7 ± 0.6
Dy	10 ± 0.5	252 ± 8	3 050 ± 90	309 ± 9	405.8 ± 9.9
Ho	2.15 ± 0.08	55 ± 4	640 ± 50	74 ± 5	85.9 ± 5.5
Er	14 ± 0.8	251 ± 16	1 850 ± 120	212 ± 14	278.9 ± 13.7
Y	75 ± 5.7	1900 ± 200	19 000 ± 2 000	2 300 ± 300	2 630.9 ± 222.3
Tm	2.12 ± 0.10	41.1 ± 1.5	241 ± 9	28.0 ± 1.0	39.0 ± 1.0
Yb	28 ± 2.2	277 ± 17	1 470 ± 90	210 ± 13	254.7 ± 10.9
Lu	7 ± 0.3	67 ± 4	220 ± 14	35 ± 2	47.1 ± 2.0

–, below detection limit.
cpx, clinopyroxene; ol, olivine; opx, orthopyroxene

tion to the occurrence of spinel, which was not decomposed using the present decomposition procedure (see Methods). In mantle rocks, the spinel often incorporates minor and trace amounts of lithophilic trace elements such as a HFSE (Bodinier *et al.* 1996; Kalfoun *et al.* 2002). The lack of spinel in the whole rock might cause the negative anomaly in HFSE in the whole rock pattern. We analyzed trace elements of the spinel in samples Ilc-1 and Sv-1 using LA–ICP–MS. Laser yield was quantified through normalization using ^{53}Cr. As a result, no trace element exceeds the detection limits (up to several tens of ppb). That is, the present spinel is negligible for the trace element budget of the xenoliths. It is therefore reasonable to consider that the HFSE depletion in the whole-rock pattern of sample Sv-1 results from the existence of other materials, such as an intergranular component, which are poor in Rb, Th, Ce, Sr, and HFSE.

TRACE ELEMENTS IN LASER-ABLATED SAMPLES

To distinguish the distribution of the material depleted in Rb, Th, Ce, Sr, and HFSE, we analyzed *in situ* trace element compositions of five spots in a clinopyroxene from sample Sv-1 using LA–ICP–MS (Fig. 6). Two spots (a, c in Fig. 6) were ablated along with trails of melt inclusions, indicating that the melt inclusions have a significant effect on the trace element compositions, especially on U content. This effect arises from the wide contrast in U contents between the clinopyroxene (<100 ppb) and the melt inclusion (more than several hundred ppb). A data table for the laser-ablation analyses is not shown because we can not correct the interelement fractionation (see Methods). Figure 7 shows a result of a line scanning analysis of trace elements for sample Sv-1. No fraction with high U content exists within the mineral matrix. The U content changes concomitant with the Ce anomaly. Dispersion of U contents in Figure 6 is caused by the mixing of the melt inclusion, as presumed before. High U contents of acid-leached minerals and slight negative anomaly in Ce in acid-leached orthopyroxene were attributable to the same cause.

Figure 8 shows trace element patterns for the intergranular component and melt inclusions

Table 3 Trace element abundance (ppb) of mineral separates and whole rock of a mantle-derived xenolith (Sv-1)

Sample					Sv-1			
Mineral	ol	opx	opx (replicate)	cpx	cpx (replicate)	Whole rock	Whole rock (replicate)	Whole rock (calculated)
Rb	112 ± 11	142 ± 14	121 ± 8	310 ± 30	142 ± 10	206 ± 20	146 ± 10	146 ± 9
Pb	–	–	7.7 ± 0.6	65 ± 5	67 ± 5	310 ± 30	280 ± 20	9 ± 1
U	16.9 ± 1.0	14.9 ± 0.8	23 ± 2	188 ± 11	95 ± 9	101 ± 6	143 ± 14	39.7 ± 2
Th	–	–	4.2 ± 0.4	9.1 ± 0.5	18.4 ± 1.5	7.8 ± 0.5	12.2 ± 1.0	1 ± 0
Ba	–	146 ± 3	330 ± 20	2 380 ± 60	1 390 ± 90	5 660 ± 140	7 000 ± 500	356 ± 8
Nb	19.9 ± 7	42 ± 4	32 ± 2	480 ± 40	164 ± 11	260 ± 20	265 ± 18	87 ± 6
Ta	0.130 ± 0.012	4.9 ± 0.5	6.2 ± 0.4	15.8 ± 1.5	23.8 ± 1.7	5.8 ± 0.5	7.2 ± 0.5	3.3 ± 0.2
La	2.00 ± 0.04	6.20 ± 0.12	11.3 ± 0.4	979 ± 19	880 ± 30	3 540 ± 70	4 220 ± 140	135 ± 3
Ce	–	11.6 ± 0.3	15.9 ± 0.5	3 480 ± 80	3 260 ± 90	1 000 ± 20	1 040 ± 30	474 ± 11
Pr	0.281 ± 0.003	3.22 ± 0.04	3.44 ± 0.10	699 ± 8	660 ± 19	476 ± 6	528 ± 15	95.6 ± 1.1
Sr	220 ± 20	470 ± 50	340 ± 60	73 000 ± 8 000	69 000 ± 12 000	19 000 ± 2 000	20 000 ± 3 000	10 100 ± 1 100
Nd	1.567 ± 0.013	22.77 ± 0.19	15.2 ± 0.7	4 130 ± 40	3 900 ± 170	2 156 ± 18	2 400 ± 100	566 ± 5
Hf	0.0195 ± 0.0016	43 ± 4	50 ± 3	930 ± 80	960 ± 50	157 ± 13	167 ± 9	136 ± 11
Zr	21.6 ± 1.9	1090 ± 90	1010 ± 90	33 000 ± 3 000	32 000 ± 3 000	5 500 ± 500	4 700 ± 400	4 700 ± 400
Sm	0.410 ± 0.004	12.37 ± 0.14	13.1 ± 1.0	1 707 ± 19	1 750 ± 130	507 ± 6	560 ± 40	234 ± 3
Eu	–	7.47 ± 0.15	7.20 ± 0.19	702 ± 14	689 ± 18	184 ± 4	224 ± 6	97 ± 2
Gd	–	28.0 ± 0.6	19.2 ± 0.7	2 400 ± 50	2 700 ± 100	726 ± 14	860 ± 30	332 ± 7
Tb	–	9.2 ± 0.3	10.4 ± 0.2	505 ± 19	514 ± 11	131 ± 5	148 ± 3	71 ± 3
Dy	2.67 ± 0.13	97 ± 5	118 ± 4	3 340 ± 170	3 460 ± 120	800 ± 40	860 ± 30	480 ± 20
Ho	0.89 ± 0.05	29.4 ± 1.8	36.0 ± 1.3	730 ± 40	780 ± 30	184 ± 11	207 ± 8	106 ± 5
Er	4.0 ± 0.3	119 ± 8	134 ± 8	2 210 ± 140	2 370 ± 140	560 ± 40	640 ± 40	329 ± 19
Y	24 ± 3	870 ± 100	850 ± 70	22 000 ± 3 000	20 900 ± 1 600	6 900 ± 800	7 000 ± 500	3 200 ± 400
Tm	0.50 ± 0.03	25.1 ± 1.6	29.9 ± 1.4	310 ± 19	326 ± 15	78 ± 5	82 ± 4	48 ± 3
Yb	9.3 ± 0.6	209 ± 14	202 ± 8	2 000 ± 140	2 110 ± 80	480 ± 30	540 ± 20	325 ± 19
Lu	2.15 ± 0.17	42 ± 3	41.5 ± 1.7	280 ± 20	288 ± 12	76 ± 6	71 ± 3	49 ± 3

–, below detection limit.

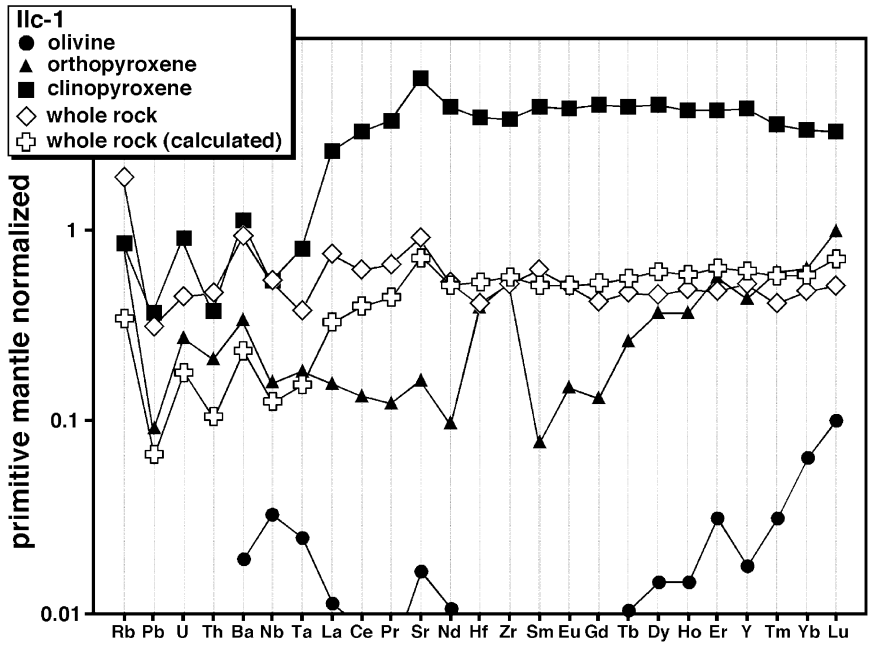

Fig. 3 Primitive mantle-normalized trace element patterns for constituent minerals and whole rock of a xenolith of sample Ilc-1. The abundance of incompatible elements in the xenolith normalized to the primitive mantle (McDonough & Sun 1995) is arranged in a sequence that reflects the incompatibility of these elements in the peridotite melt system. Trace element pattern for whole rock calculated by the mineral mode of the constituent minerals and trace element compositions of the acid-leached minerals are also shown.

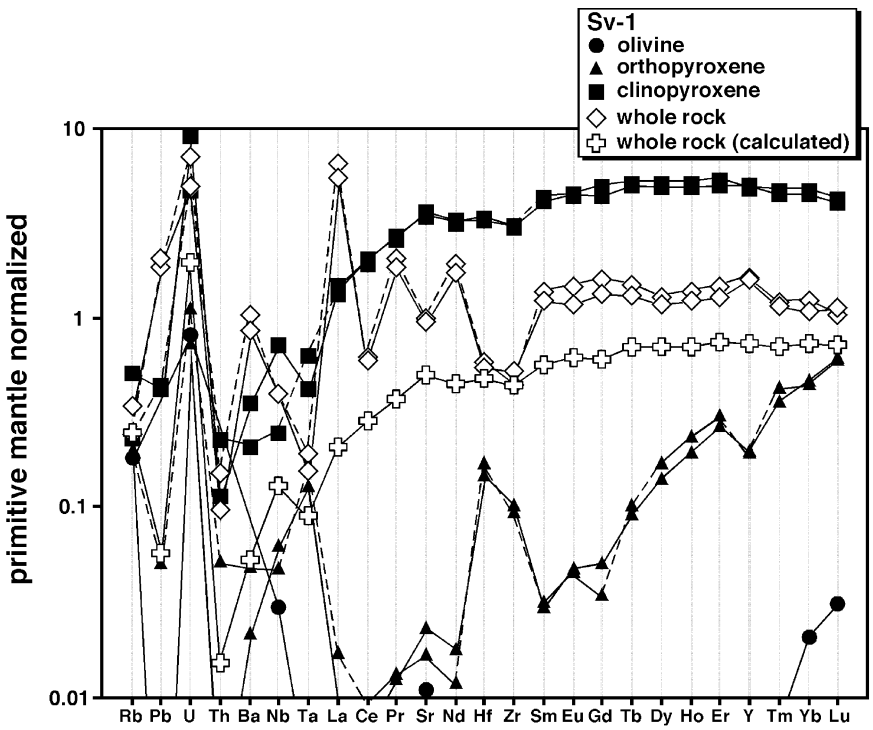

Fig. 4 Primitive mantle-normalized trace element patterns for constituent minerals and whole rock of a xenolith of sample Sv-1. Analyses were duplicated separately for orthopyroxene, clinopyroxene, and whole rocks. The trace element pattern for the whole rock calculated using the mineral mode of the constituent minerals and trace element compositions of the acid-leached minerals are also shown.

accompanied by the pattern for the analyzed whole rock. Both the intergranular component and the melt inclusions show negative anomalies in Rb, Th, Ce, Sr, and HFSE. The intergranular component and the melt inclusions are causative agents for the anomalies observed in the whole rock of sample Sv-1.

DISCUSSION

DISTRIBUTION OF MATERIAL DEPLETED IN Rb, Th, Ce, Sr, AND HFSE

The present results show whole rock compositions of incompatible trace elements that are larger than

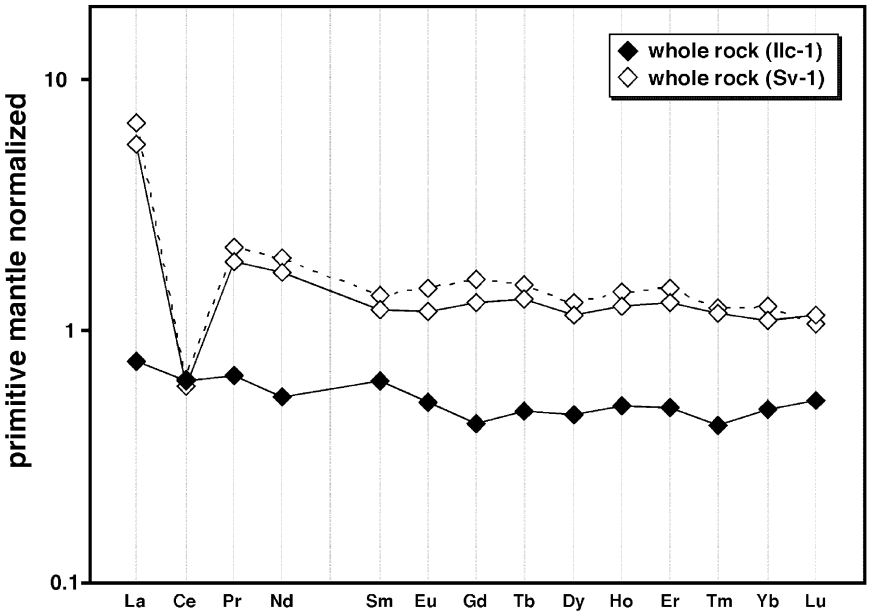

Fig. 5 Primitive mantle-normalized rare earth element patterns for whole rocks of xenoliths of samples IIc-1 and Sv-1.

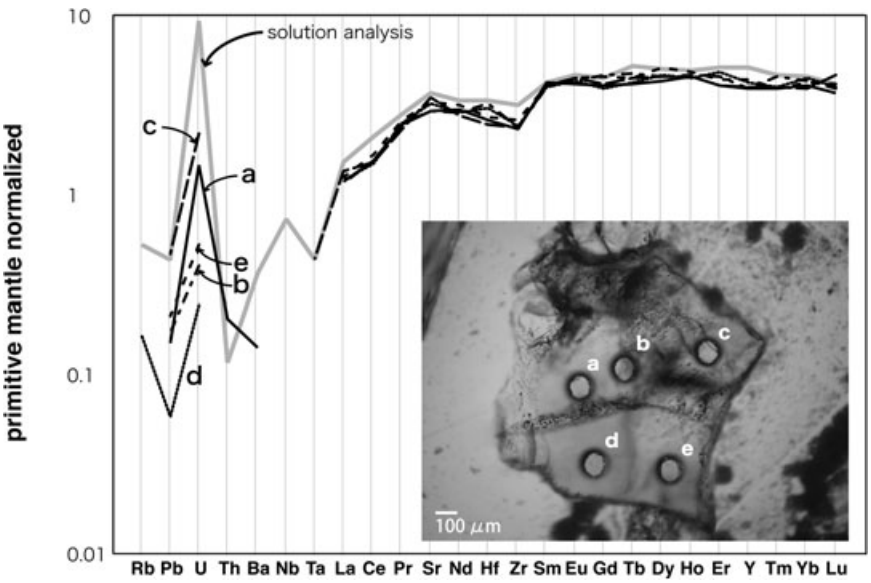

Fig. 6 Primitive mantle-normalized trace element patterns for clinopyroxene in sample Sv-1, as analyzed using LA–ICP–MS, accompanied by data obtained from solution analysis. Analyses using LA–ICP–MS were repeated five times. Analyzed points are indicated as a–e in the photograph. Ablated materials from two spots (a, c) involved melt inclusions.

expected based on results of analyses of the acid-leached mineral grains in the rocks, especially for highly incompatible elements (Figs 3,4). Such a discrepancy requires storage of the incompatible trace elements in intergranular areas of the rocks. Many mantle xenoliths are known to contain veins and patches of glass (Frey & Prinz 1978; Wirth 1996; Yaxley *et al.* 1997; Yaxley & Kamenetsky 1999; Coltorti *et al.* 2000; Xu *et al.* 2003; Ishimaru *et al.* 2006). Suzuki (1987) assumed that the intergranular component is a thin quenched glass, with thickness of a few tens of nanometers at most. Wirth (1996) observed 1 to 2-nm-thick intergranular amorphous films in some mantle xenoliths using high-resolution transmission electron microscopy (HRTEM). Hiraga *et al.* (2007) reported that segregation of incompatible elements at grain interfaces leads to the formation of an interface segregation region with thickness of 0.7 to 0.8 nm in some polycrystalline oxides based on analyses using HRTEM. The present intergranular component would also be such a thin intergranular component because the intergranular enrichment of the incompatible elements was removed easily by washing in a mild acid solution. Figure 9 presents a comparison of trace element compositions between the whole rocks and the calculated whole rocks, which is helpful to show the

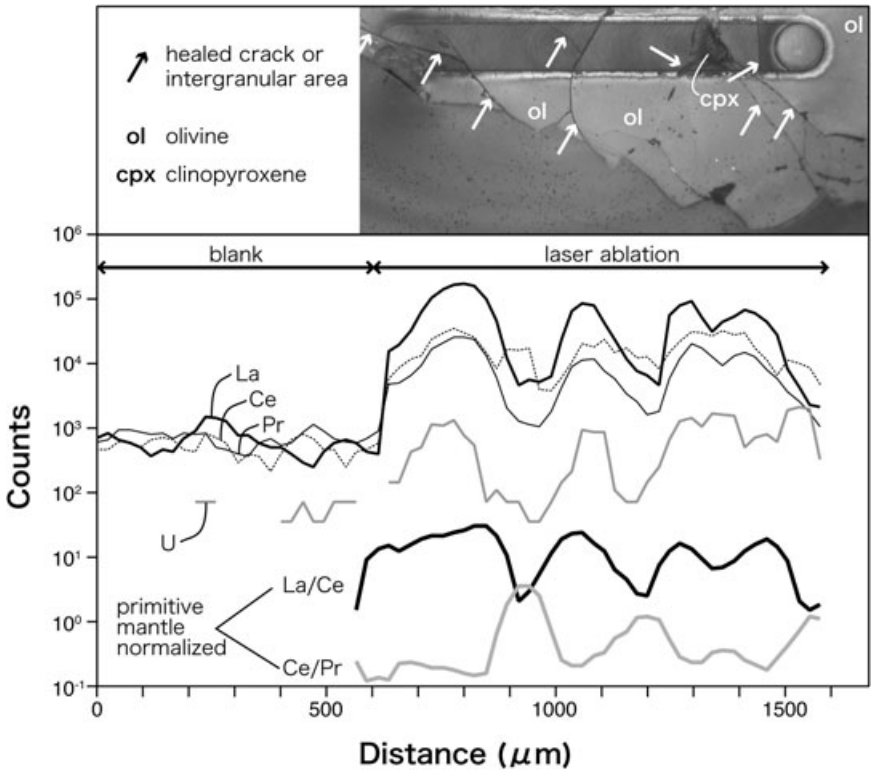

Fig. 7 Result of line analysis of sample Sv-1 using LA–ICP–MS. The laser beam traverses many intergranular areas and healed cracks in the mantle xenolith, which are indicated by arrows in the photograph. The healed cracks and melt inclusions look alike. A new generation of melt inclusions along the healed cracks was observed. The healed cracks often crosscut grain boundaries. The material derived from the intergranular areas and healed cracks shows high U content and apparent negative anomaly in Ce.

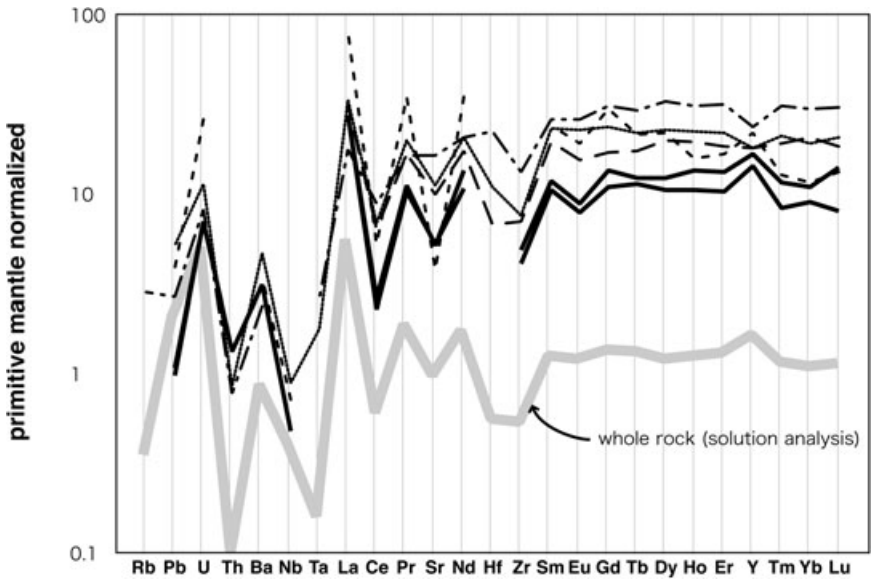

Fig. 8 Primitive mantle-normalized trace element patterns for melt inclusions (solid lines) and intergranular components (broken lines) in sample Sv-1 analyzed using LA–ICP–MS, accompanied by data of analyzed whole rock.

trace element composition of the intergranular component. The contents of highly incompatible elements of the analyzed whole rocks tend to be higher than those of the calculated whole rocks. The U contents of acid-leached minerals for sample Sv-1 are affected by the intergranular component and the melt inclusions, as shown in Figures 6 and 7. Therefore, the intergranular component for sample Sv-1 would have spikes of U, Ba, and La, and depleted Rb, Th, Ce, Sr, and HFSE, but that for sample Ilc-1 would show simple enrichment of highly incompatible elements.

The same trace element pattern as that of the analyzed whole rock for sample Sv-1 was obtained from both the intergranular component and the melt inclusion analyzed using LA–ICP–MS (Fig. 8). This result indicates that the intergranu-

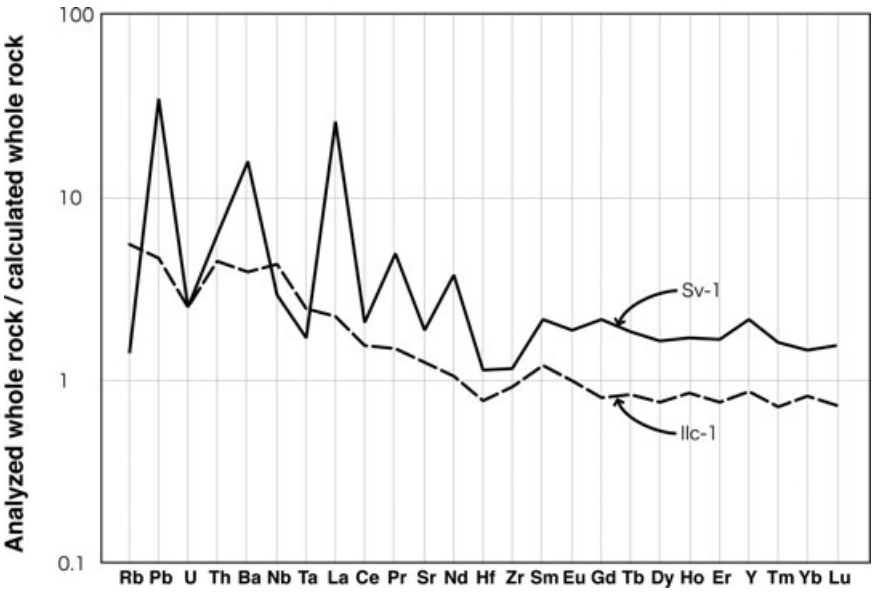

Fig. 9 Trace element patterns for analyzed whole rocks, normalized using calculated whole rock data.

lar component and the melt inclusion are important host phases of the trace elements in the mantle xenolith. Hiraga *et al.* (2004, 2007) predicted that elements with ionic radius (or incompatibility) larger than Sr will mostly remain at grain boundaries, which might be apparent in sample Ilc-1 (Fig. 9). Such enrichment of the incompatible elements with large ionic radii along intergranular areas in mantle xenoliths was detected using LA–ICP–MS (Ishimaru *et al.* 2006). For sample Sv-1, enrichment of incompatible elements at the intergranular area relative to the grain matrices does not, however, occur parallel to the incompatibility of the elements, which indicates that the anomalies are initial properties of the intergranular component. Thus, a metasomatizing fluid or melt located as the intergranular component is responsible for whole-rock inventory of incompatible trace elements for sample Sv-1, rather than interface segregation.

Occurrence of the intergranular component in the mantle xenoliths from this region was earlier indicated from trace element data of whole rocks and clinopyroxenes (Ionov *et al.* 1995; Kalfoun *et al.* 2002). Ionov *et al.* (1995) found negative Ce anomalies in the whole-rock patterns of the mantle xenoliths from this region and, because of the absence of the anomalies in the clinopyroxene, concluded that the anomalies are hosted by the intergranular component. In the present study, we obtained identical trace element patterns from the melt inclusion and the intergranular component. Trace elements in the intergranular component might be affected by infiltration of host magma or weathering near the Earth's surface. Therefore, the trace element patterns of melt inclusions in mantle-derived minerals are useful to identify geochemical features of mantle fluid. Analyses of trace elements using LA–ICP–MS in the present work must first give certain proof for that inference made by Ionov *et al.* (1995).

Results of the present study show that the intergranular component has an uncertain effect on the trace element composition of mantle xenoliths even where trace element characteristics of whole rock are likely to be explained using the sum of constituent minerals. For example, the high contents of highly incompatible trace elements (Rb–Ta) of sample Ilc-1 are inexplicable by the sum of constituent minerals in sample Ilc-1 (Fig. 9). This fact is indicative of the occurrence of the intergranular component in sample Ilc-1, as is true with sample Sv-1. Comparison of trace element compositions between the whole rock and acid-leached minerals enables estimation of the respective contributions of minerals and the intergranular component (Fig. 10). For sample Ilc-1, highly incompatible elements in the intergranular component contribute to the trace element composition of the whole rock resulting from interface segregation of the trace elements, as predicted by Hiraga *et al.* (2004, 2007). Sample Sv-1 also has a contribution of the intergranular component but does not show simple correlation with incompatibility, which implies the exotic origin of the intergranular component as with the melt inclusions.

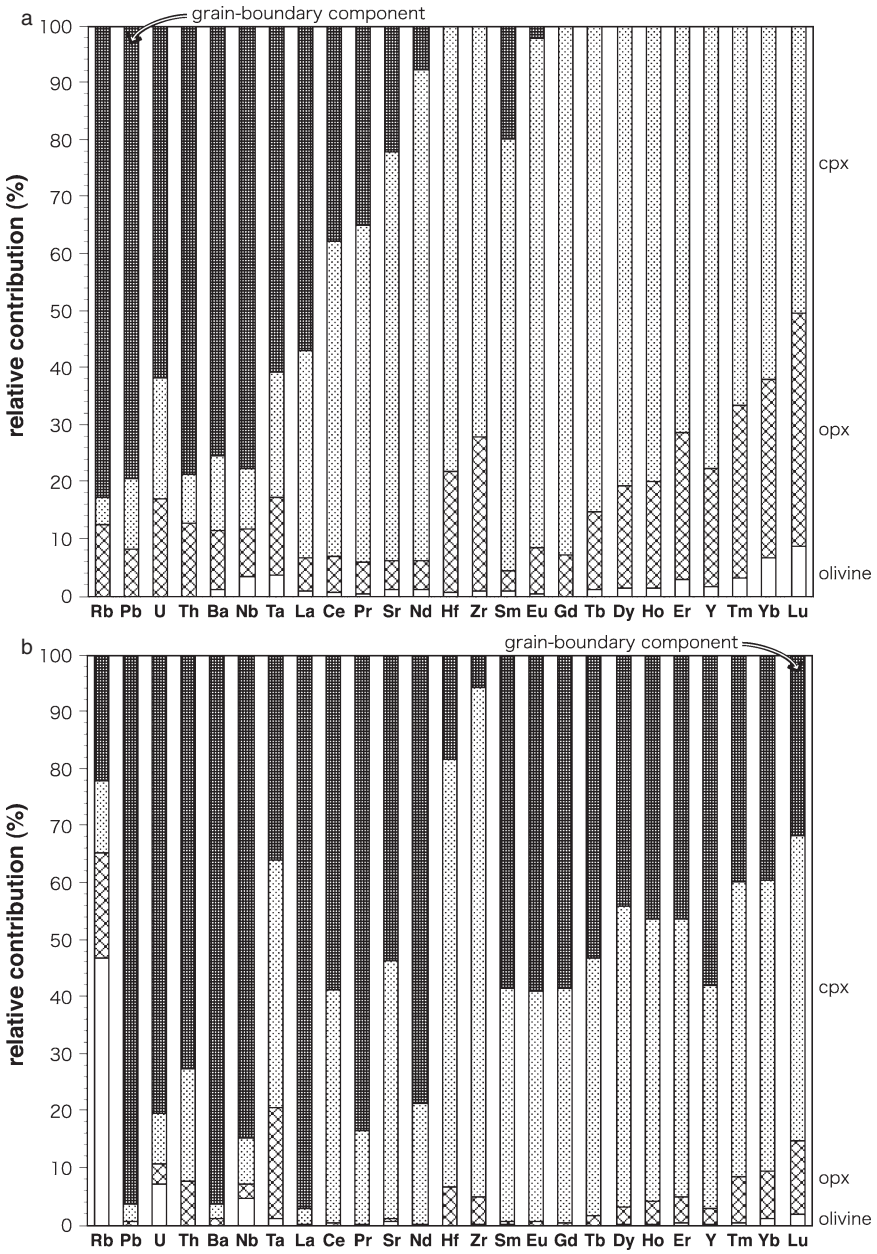

Fig. 10 Relative contributions of constituent minerals and the intergranular component to the trace element composition of whole rock for several trace elements in (a) sample IIc-1, and (b) sample Sv-1.

POSITIVE ANOMALIES AMONG SOME HIGHLY INCOMPATIBLE ELEMENTS

Olivine and orthopyroxene are moderately depleted in highly incompatible elements (Pb–Nd). They do not play important roles in characterizing the whole rock in the incompatible trace element compositions (Fig. 10). However, the total contribution of olivine and orthopyroxene to the Rb content of the whole rock for sample Sv-1 is not small. Such a state would result from mixing of the melt inclusion or the intergranular component, as evidenced by the fact that all mineral species in sample Sv-1 show nearly equal Rb contents, and that the reproducibility of duplicate analyses was quite variable (Table 3, Fig. 4). However, we were unable to obtain direct evidence of high Rb content in the intergranular component and the melt inclusion using LA–ICP–MS because of its high detection limit, several hundred parts per billion (Figs 6,8). Similarly, the contribution of olivine to U content in sample Sv-1 is an important concern (Fig. 10b). Although positive U anomalies in constituent minerals from mantle xenoliths have also been reported (Ionov *et al.* 1995; Bedini & Bodinier 1999), the olivine in sample Sv-1 contains around 20 times more U than olivine in samples from the same area reported by Ionov *et al.* (1995).

The present olivine shows relative abundance of U, similar to that in clinopyroxene, in spite of the fact that the concentrations of most elements in olivine are about an order of magnitude lower than those in the clinopyroxene. That high U content is attributable to imperfect acid leaching or existence of a U-rich melt inclusion, as shown in Figures 6–8.

Overall, the whole rock of sample Sv-1 reveals a nearly flat REE pattern with depletion in Rb, Th, Ce, Sr, and HFSE, and spikes of U, Ba, and La (Fig. 4). This might indicate at least a two-stage history for the xenolith. Depletions in highly incompatible elements can be induced by the loss of a partial melt enriched in the incompatible elements. Spikes of U, Ba, and La in the whole rock pattern suggest that the depletion event was followed by an enrichment episode involving a material that is rich in U, Ba, and La, but very poor in Rb, Th, Ce, Sr, and HFSE. That conjecture is plausible. Although the constituent minerals of sample Sv-1 are markedly enriched in U, they have depleted patterns with a gradual decrease in LREE and low values of highly incompatible elements. On the other hand, the intergranular component and the melt inclusion in sample Sv-1 have spikes of U, Ba, and La. These spikes are consistent with an interpretation that the high contents of U, Ba, and La in the whole rock exist largely because of a depletion event and a subsequent enrichment event.

NATURE OF METASOMATIZING AGENT

We can rule out a post eruption surface alteration as an origin for the anomalies on the normalized trace element patterns of sample Sv-1 because we detected trace element patterns of the melt inclusions similar to those of intergranular component. Trace elements in melt inclusions in mantle xenoliths are isolated during transport of the mantle xenolith and subsequent cooling. Therefore, the anomalies in the trace element patterns of the melt inclusions reflect an inherent feature of metasomatizing melt or fluid in the mantle.

The trace element pattern of the intergranular component and the melt inclusions in sample Sv-1 is mainly characterized by great depletion of Th, Ce, and HFSE. Kalfoun *et al.* (2002) explained the negative Ce anomaly by La-inflection in metasomatized mantle rocks that were produced by adding small amounts of LREE-rich fluid to LREE-depleted mantle rocks. It is, however, obvious that the negative Ce anomaly in the present study can not be explained by the above process (Fig. 5). The Ce anomaly may be developed by oxidation of Ce^{3+} to Ce^{4+}. The change in ionic charge and radius engenders decoupling of Ce^{4+} from trivalent REEs (except for Eu). For that reason, the negative Ce anomaly indicates a process associated with generation of Ce^{4+} in an oxidizing condition. The negative Ce anomalies of mantle rocks are attributable to the same cause as that in HFSE. Many studies considered that the negative anomalies in HFSE of mantle rocks are related to the low solubility of HFSE in aqueous solutions. Cerium is not soluble much in the aqueous fluid caused by generation of Ce^{4+} (Henderson 1984). The same would be said of Th. Some xenoliths from far eastern Russia show Th/U ratios that are much lower than those of the mantle (Fig. 11). Such low Th/U ratios would be explained by fractionation between Th and U. Many papers related to U–Th dating of volcanic rocks have presented conjectures on fractionation by the difference in their solubilities in aqueous fluid. As described above, the high U content resulting in low Th/U ratios is attributable to the existence of the intergranular component and the melt inclusion. From this point of view, it is noteworthy that hydrous minerals were observed on the wall of the melt inclusions in sample Sv-1, which is indicative of the occurrence of a melt with a considerable amount of water in the mantle beneath paleo-far eastern Russia (Fig. 2a). Consequently, we conclude that the aqueous fluid is concerned in

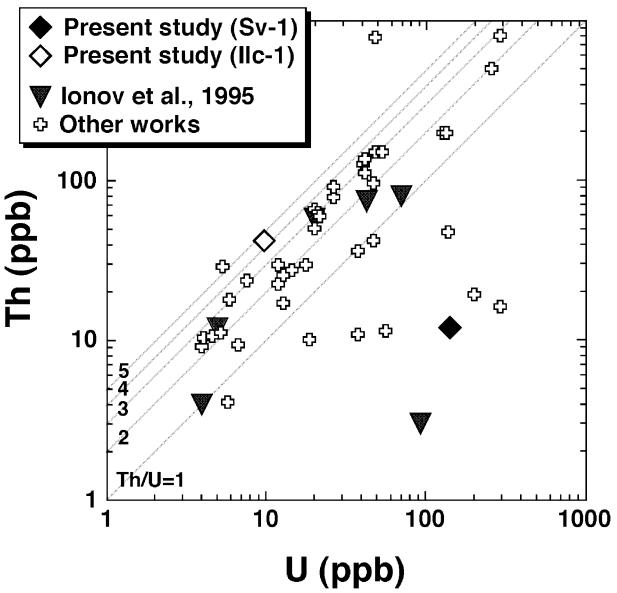

Fig. 11 Concentrations of U *vs* Th from the ultramafic rocks. Data from Wakita *et al.* (1967) and Tolstikhin *et al.* (1974) are referenced. The Th/U in the mantle is inferred to be about 4 (Jochum *et al.* 1983; Staudacher *et al.* 1989).

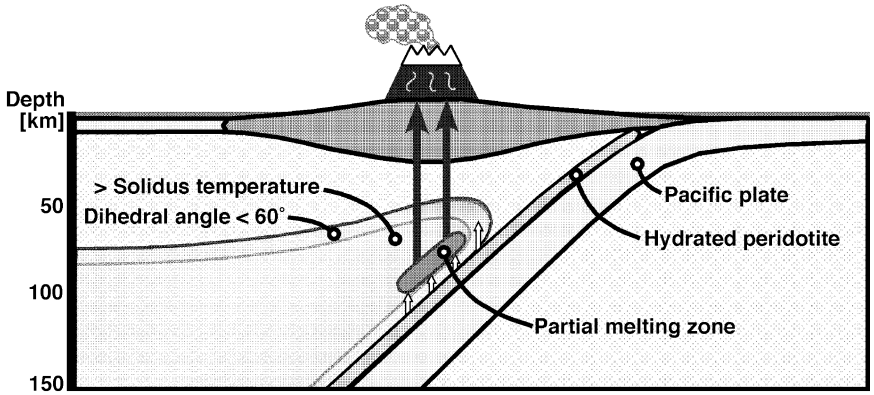

Fig. 12 Schematic cross-section beneath the paleo-far eastern Russia.

generation of the intergranular component and the melt inclusion in sample Sv-1.

RESPECTIVE ORIGINS OF INTERGRANULAR COMPONENTS AND MELT INCLUSIONS

Lastly, in this section we consider a possible origin of the intergranular component and the melt inclusions. Isotopic data of Li–Sr–Nd of the mantle xenoliths from far eastern Russia, including the sample Sv-1, were reported by bulk analysis of clinopyroxene separates (Nishio *et al.* 2004). Regarding the Li isotope data, recent studies reported Li isotope zonation in minerals in mantle xenoliths attributed to diffusion of Li from host magma (Jeffcoate *et al.* 2007; Rudnick & Ionov 2007; Ionov & Seitz 2008). Thus, intermineral disequilibria is the point to be specially considered when an extreme Li isotopic ratio was detected as shown in Nishio *et al.* (2004) by bulk analyses of mineral separates. Therefore, we do not consider the Li isotope systematics in the present discussion. Nishio *et al.* (2004) reported that the $^{143}Nd/^{144}Nd$ negatively correlated with $^{87}Sr/^{86}Sr$. This feature was explained by the results of binary mixing between a depleted component (high $^{143}Nd/^{144}Nd$, low $^{87}Sr/^{86}Sr$) and an enriched component (EM-1 type source: low $^{143}Nd/^{144}Nd$, high $^{87}Sr/^{86}Sr$), indicating that a metasomatizing agent related to the subducted slab affected the lithospheric mantle beneath this region. Yamamoto *et al.* (2004) inferred the occurrence of melt inclusions with high U content in sample Sv-1 from extremely low $^{3}He/^{4}He$ in the melt inclusions, which is strikingly consistent with the present result. In addition, considering atmospheric $^{40}Ar/^{36}Ar$ in the melt inclusions, they speculated that the melt inclusion is melt-derived from a partial melting zone in the mantle wedge beneath paleo-far eastern Russia. Assuming a subduction environment, we can give a plausible reason for the occurrence of aqueous fluid in the melt inclusions and the intergranular component.

Figure 12 shows a schematic cross-section of the region beneath paleo-far eastern Russia. The oceanic lithosphere subducts into the mantle wedge. Beneath the continental active margin or island arc, aqueous fluid derived from the subducted slab ascends into the mantle wedge. Hydrated peridotite was formed by the addition of slab-derived H_2O. Hydrous minerals such as amphibole, chlorite, and phlogopite in the hydrated peridotite broke down in the downward flow of the mantle wedge and released H_2O. Interconnection of the aqueous fluid in the hydrated peridotite is determined by dihedral angles of mineral grains. At low pressure and temperature, most aqueous fluids generated by successive decomposition of the hydrous minerals in downdragged hydrous peridotite could not segregate from solids and were instead transported to greater depths as free fluid in isolated pores among minerals. If such downdragged hydrous peridotite reaches a region where the dihedral angle is less than 60°, aqueous fluid is supplied continuously from the downdragged hydrous peridotite (Mibe *et al.* 1998, 1999). Partial melting in the mantle wedge took place to produce initial magma when the aqueous fluid reached the region with the solidus temperature of hydrous peridotite. If the aqueous fluid detours, avoiding the partial melting zone (the rightmost open arrow in Fig. 12), it infiltrates directly into the mantle located above the partial melting zone. It eventually forms H_2O inclusions or emerges to the Earth's surface as hydrothermal fluid. Melt was extracted upwards from the partial melting zone, ascending through the mantle wedge, engendering subduction-related volcanism if melt segregation occurred. Part of the melt should remain in the

mantle wedge as intergranular components and melt inclusions.

At an active margin of a continent or an island arc, several types of fluid infiltrate the mantle wedge. For instance, aqueous fluid released from the descending oceanic lithosphere triggers partial melting of the mantle wedge. The melt subsequently ascends through the mantle wedge, leading to subduction-related volcanism. In that case, part of the melt would remain as an intergranular component or as a melt inclusion in the upper part of the mantle wedge where the present mantle xenoliths were derived (35 to 43 km). The melt ascended from the partial melting zone contains features of depletion in Th, Ce, and HFSE, as described previously. In this respect, the depletion in Th, Ce, and HFSE in the intergranular component and the melt inclusions of the present xenoliths is a key result.

However, some problems remain to connect the origin of the intergranular component and the melt inclusions in the present mantle xenoliths to the subduction-related material. For example, the negative anomaly in Ce and/or anomalies of Th, U, and HFSE alone can not be considered valid indices of subduction-related origin of mantle-derived materials (Ionov *et al.* 1995). Anomalies of Th, U, and HFSE are common in intra-plate mantle xenoliths (Ionov *et al.* 2006). The negative anomaly in Ce was also observed in intra-plate mantle xenoliths from eastern Asia: southeast China (Xu *et al.* 2003) and north China (Tang *et al.* 2008). In addition, the present data show decoupled U–Pb and Sr spikes on the trace element patterns for the intergranular component and the melt inclusions, which is unusual for arc-related volcanic rocks. Hence, it is still unclear at this stage whether the intergranular component and the melt inclusions have a relation to the subduction system in their generation. Accumulation of trace element data of intergranular components and melt inclusions in mantle wedge-derived xenoliths will be necessary to evaluate the significance of the present data.

CONCLUSION

1. The whole-rock trace element pattern for sample Ilc-1 is dominated by that of clinopyroxene and an intergranular component possibly resulting from interface segregation. The trace element pattern of the whole rock for sample Sv-1 shows great depletion of Rb, Th, Ce, Sr, and HFSE. Such anomalies are not so apparent among acid-leached constituent minerals, and they do not show simple correlation with incompatibility of elements, thereby suggesting the contribution of an exotic intergranular component.
2. The melt inclusions have the same trace element pattern as that of the intergranular component of sample Sv-1, which is direct evidence supporting the occurrence of an exotic fluid in the mantle beneath far eastern Russia. Furthermore, similarity of the trace element pattern between whole rock and the melt inclusions indicates a significant contribution of the exotic mantle fluid to the inventory of the trace elements in a part of the far eastern Russian mantle.
3. Low Th/U and depletion in Ce and HFSE in the trace element pattern of the intergranular component and the melt inclusions indicate a relation to aqueous fluid in their origin. Hydrous melt inclusions were observed in sample Sv-1. Therefore, the trace element compositions of the intergranular component and the melt inclusions afford an example for aqueous fluid-related metasomatizing agent.

ACKNOWLEDGEMENTS

We appreciate constructive reviews from D. A. Ionov and T. Hiraga that improved the manuscript. We thank Y. Ishida, Y. Lai, Y. V. Sahoo, Y. Nishio, S. Fukuda, Y. Maeda, R. Tatsuta, S. Tokunaga, and Y. Watanabe for assistance in trace elements analysis using ICP–MS. We appreciate helpful suggestions and assistance related to major element analyses offered by T. Koyaguchi, A. Yasuda, C. Gouzu, and M. Yamada. We also thank M. D. Kurz, N. Shimizu, T. Hanyu, Y. Nishio, H. Sumino, and M. Sasaki for valuable comments and criticism of this study. Particularly, S.A. is indebted to S. A. Shcheka, S. V. Nechaev, and M. Sasaki for help in the field. This study was financially supported in part by Research Fellowships for Young Scientists and Postdoctoral Fellowship for Research Abroad of Japan Society of Promotion of Science (JSPS), and a Grant-in-Aid from the 21st Century COE Program (Kyoto University, G3) to J.Y., and Grants-in-Aid for Scientific Research from the Ministry of Education, Culture, Sports, Science and Technology in Japan to I.K. (Nos. 09440182, 09954023, and 12440145).

REFERENCES

ARAI S. 1994. Characterization of spinel peridotites by olivine-spinel compositional relationships: Review and interpretation. *Chemical Geology* **113**, 191–204.

BEBOUT G. E., BEBOUT A. E. & GRAHAM C. M. 2007. Cycling of B, Li, and LILE (K, Cs, Rb, Ba, Sr) into subduction zones: SIMS evidence from micas in high-P/T metasedimentary rocks. *Chemical Geology* **239**, 284–304.

BEDINI R. M. & BODINIER J.-L. 1999. Distribution of incompatible trace elements between the constituents of spinel peridotite xenoliths: ICP-MS data from the East African Rift. *Geochimica et Cosmochimica Acta* **63**, 3883–900.

BENCE A. E. & ALBEE A. L. 1968. Empirical correction factors for the electron microanalysis of silicates and oxides. *Journal of Geology* **76**, 382–403.

BODINIER J.-L., MERLET C., BEDINI R. M. *et al.* 1996. Distribution of niobium, tantalum and other highly incompatible trace elements in the lithospheric mantle: The spinel paradox. *Geochimica et Cosmochimica Acta* **60**, 545–50.

COLTORTI M., BECCALUBA L., BONADIMAN C. *et al.* 2000. Glasses in mantle xenoliths as geochemical indicators of metasomatic agents. *Earth and Planetary Science Letters* **183**, 303–20.

DALTON J. A. & PRESNALL D. C. 1998. The continuum of primary carbonatitic-kimberlitic melt compositions in equilibrium with lherzolite: Data from the system CaO-MgO-Al_2O_3-SiO_2-CO_2 at 6GPa. *Journal of Petrology* **39**, 1953–64.

ESIN S. V. & TRAVIN A. V. 1994. Xenolith-bearing alkali basaltoids of central Sikhote-Alin. *Russian Geology Geophys* **35**, 61–71.

FAN Q. & HOOPER P. R. 1989. The mineral chemistry of ultramafic xenoliths of eastern China: Implications for upper mantle composition and the paleogeotherms. *Journal of Petrology* **30**, 1117–58.

FAURE M. & NATAL'IN B. A. 1992. The geodynamic evolution of the eastern Eurasian margin in Mesozoic times. *Tectonophysics* **208**, 397–411.

FAURE M., NATAL'IN B. A., MONIÉ P. *et al.* 1995. Tectonic evolution of the Anuy metamorphic rocks (Sikhote Alin, Russia) and their place in the Mesozoic geodynamic framework. *Tectonophysics* **241**, 279–301.

FEINEMAN M. D., RYERSON F. J., DEPAOLO D. J. *et al.* 2007. Zoisite-aqueous fluid trace element partitioning with implications for subduction zone fluid composition. *Chemical Geology* **239**, 250–65.

FREY F. A. & PRINZ M. 1978. Ultramafic inclusions from San Carlos, Arizona: Petrologic and geochemical data bearing on their petrogenesis. *Earth and Planetary Science Letters* **38**, 129–76.

HENDERSON P. 1984. *Rare Earth Element Geochemistry*. Elsevier, Amsterdam.

HIRAGA T., ANDERSON I. M. & KOHLSTEDT D. L. 2004. Grain boundaries as reservoirs of incompatible elements in the Earth's mantle. *Nature* **427**, 699–703.

HIRAGA T., HIRSCHMANN M. M. & KOHLSTEDT D. L. 2007. Equilibrium interface segregation in the diopside-forsterite system II: Applications of interface enrichment to mantle geochemistry. *Geochimica et Cosmochimica Acta* **71**, 1281–9.

IONOV D. A. & SEITZ H.-M. 2008. Lithium abundances and isotopic compositions in mantle xenoliths from subduction and intra-plate settings: Mantle sources vs. eruption histories. *Earth and Planetary Science Letters* **266**, 316–31.

IONOV D. A., CHAZOT G., CHAUVEL C. *et al.* 2006. Trace element distribution in peridotite xenoliths from Tok, SE Siberian craton: A record of pervasive, multi-stage metasomatism in shallow refractory mantle. *Geochimica et Cosmochimica Acta* **70**, 1231–60.

IONOV D. A., PRIKHOD'KO V. S. & O'REILLY S. Y. 1995. Peridotite xenoliths in alkali basalts from the Sikhote-Alin, southeastern Siberia, Russia: Trace-element signatures of mantle beneath a convergent continental margin. *Chemical Geology* **120**, 275–94.

ISHIMARU S., ARAI S., ISHIDA Y. *et al.* 2006. Melting and multi-stage metasomatism in the mantle wedge beneath a frontal arc inferred from highly depleted peridotite xenoliths from the Avacha volcano, southern Kamchatka. *Journal of Petrology* **48**, 395–433.

ISHIWATARI A. & TSUJIMORI T. 2003. Paleozoic ophiolites and blueschists in Japan and Russian Primorye in the tectonic framework of East Asia: A synthesis. *Island Arc* **12**, 190–206.

JEFFCOATE A. B., ELLIOTT T., KASEMANN S. A. *et al.* 2007. Li isotope fractionation in peridotites and mafic melts. *Geochimica et Cosmochimica Acta* **71**, 202–18.

JOCHUM K. P., HOFMANN A. W., ITO E. *et al.* 1983. K, U and Th in mid-ocean ridge basalt glasses and heat production, K/U and K/Rb in the mantle. *Nature* **306**, 431–6.

KALFOUN F., IONOV D. & MERLET C. 2002. HFSE residence and Nb/Ta ratios in metasomatised, rutile-bearing mantle peridotites. *Earth and Planetary Science Letters* **199**, 49–65.

KAWAKAMI Y., YAMAMOTO J. & KAGI H. 2003. Micro-Raman densimeter for CO_2 inclusions in mantle-derived minerals. *Applied Spectroscopy* **57**, 1333–9.

KEPEZHINSKAS P. K., DEFANT M. J. & DRUMMOND M. S. 1995. Na metasomatism in the island-arc mantle by slab melt-peridotite interaction; evidence from mantle xenoliths in the North Kamchatka arc. *Journal of Petrology* **36**, 1505–27.

KILIAN R. & STERN C. R. 2002. Constraints on the interaction between slab melts and the mantle wedge from adakitic glass in peridotitic xenoliths. *European Journal of Mineralogy* **14**, 25–36.

MCDONOUGH W. F. & SUN S.-S. 1995. The composition of the Earth. *Chemical Geology* **120**, 223–53.

McDonough W. F., Stosch H. G. & Ware N. G. 1992. Distribution of titanium and the rare earth elements between peridotitic minerals. *Contributions to Mineralogy and Petrology* **110**, 321–8.

Mibe K., Fujii T. & Yasuda A. 1998. Connectivity of aqueous fluid in the Earth's upper mantle. *Geophysical Research Letters* **25**, 1233–6.

Mibe K., Fujii T. & Yasuda A. 1999. Control of the location of the volcanic front in island arcs by aqueous fluid connectivity in the mantle wedge. *Nature* **401**, 259–62.

Nakamura Y. & Kushiro I. 1970. Compositional relations of coexisting orthopyroxene, pigeonite and augite in a tholeiitic andesite from Hakone volcano. *Contributions to Mineralogy and Petrology* **26**, 265–75.

Natal'in B. A. 1993. History and modes of Mesozoic accretion in southeastern Russia. *Island Arc* **2**, 15–34.

Nishio Y., Nakai S., Yamamoto J. *et al.* 2004. Lithium isotopic systematics of the mantle-derived ultramafic xenoliths: Implications for EM1 origin. *Earth and Planetary Science Letters* **217**, 245–61.

O'Reilly S. Y., Griffin W. L. & Ryan C. G. 1991. Residence of trace elements in metasomatized spinel lherzolite xenoliths: A proton-microprobe study. *Contributions to Mineralogy and Petrology* **109**, 98–113.

Rudnick R. L. & Ionov D. A. 2007. Lithium elemental and isotopic disequilibrium in minerals from peridotite xenoliths from far-east Russia: Product of recent melt/fluid-rock reaction. *Earth and Planetary Science Letters* **256**, 278–93.

Salters V. J. M. & Shimizu N. 1988. World-wide occurrence of HFSE-depleted mantle. *Geochimica et Cosmochimica Acta* **52**, 2177–82.

Sato K. 2000. *Cenozoic volcanism in northern Sikhote Alin, Far East Russia and its implication for the opening of the Japan Sea*. PhD Thesis, Kyoto University, Kyoto.

Spandler C., Mavrogenes M. & Hermann J. 2007. Experimental constraints on element mobility from subducted sediments using high-P synthetic fluid/melt inclusions. *Chemical Geology* **239**, 228–49.

Staudacher T., Sarda P., Richardson S. H. *et al.* 1989. Noble gases in basalt glasses from a Mid-Atlantic Ridge topographic high at 14°N: Geodynamic consequences. *Earth and Planetary Science Letters* **96**, 119–33.

Stosch H. G. 1982. Rare earth element partitioning between minerals from anhydrous spinel peridotite xenoliths. *Geochimica et Cosmochimica Acta* **46**, 793–811.

Suzuki K. 1987. Grain-boundary enrichment of incompatible elements in some mantle peridotites. *Chemical Geology* **63**, 319–34.

Tang Y. -J., Zhang H. -F., Ying J. -F. *et al.* 2008. Refertilization of ancient lithospheric mantle beneath the central North China Craton: Evidence from petrology and geochemistry of peridotite xenoliths. *Lithos* **101**, 435–52.

Tolstikhin I. N., Mamyrin B. A., Khabarin L. B. *et al.* 1974. Isotopic composition of helium in ultrabasic xenoliths from volcanic rocks of Kamchatka. *Earth and Planetary Science Letters* **22**, 75–84.

Wakita H., Nagasawa H., Uyeda S. *et al.* 1967. Uranium, thorium and potassium contents of possible mantle materials. *Geochemical Journal* **1**, 183–98.

Wells P. R. A. 1977. Pyroxene thermometry in simple and complex systems. *Contributions to Mineralogy and Petrology* **62**, 129–39.

Wirth R. 1996. Thin amorphous films (1–2 nm) at olivine grain boundaries in mantle xenoliths from San Carlos, Arizona. *Contributions to Mineralogy and Petrology* **124**, 44–54.

Xu X., O'Reilly S. Y., Griffin W. L. *et al.* 2003. Enrichment of upper mantle peridotite: Petrological, trace element and isotopic evidence in xenoliths from SE China. *Chemical Geology* **198**, 163–88.

Yamamoto J. 2007. Subduction-related fluid occurrence in mantle revealed by residual pressure and isotopic compositions of fluid inclusion. *Chikyukagaku (Geochemistry)* **41**, 63–75 (in Japanese with English abstract).

Yamamoto J. & Kagi H. 2006. Extended micro-Raman densimeter for CO_2 applicable to mantle-originated fluid inclusions. *Chemistry Letters* **35**, 610–11.

Yamamoto J. & Kagi H. 2008. Application of micro-Raman densimeter for CO_2 fluid inclusions: A probe for elastic strengths of mantle minerals. *European Journal of Mineralogy* **20**, 529–35.

Yamamoto J., Kagi H., Kaneoka I. *et al.* 2002. Fossil pressures of fluid inclusions in mantle xenoliths exhibiting rheology of mantle minerals: Implications for the geobarometry of mantle minerals using micro Raman spectroscopy. *Earth and Planetary Science Letters* **198**, 511–9.

Yamamoto J., Kagi H., Kawakami Y. *et al.* 2007. Paleo-Moho depth determined from the pressure of CO_2 fluid inclusions: Raman spectroscopic barometry of mantle- and crust-derived rocks. *Earth and Planetary Science Letters* **253**, 369–77.

Yamamoto J., Kaneoka I., Nakai S. *et al.* 2004. Evidence for subduction-related components in the subcontinental mantle from low $^{3}He/^{4}He$ and $^{40}Ar/^{36}Ar$ ratio in mantle xenoliths from Far Eastern Russia. *Chemical Geology* **207**, 237–59.

Yaxley G. M. & Kamenetsky V. 1999. In situ origin for glass in mantle xenoliths from southeastern Australia: Insights from trace element compositions of glasses and metasomatic phases. *Earth and Planetary Science Letters* **172**, 97–109.

Yaxley G. M., Kamenetsky V., Green D. H. *et al.* 1997. Glasses in mantle xenoliths from western Victoria, Australia, and their relevance to mantle processes. *Earth and Planetary Science Letters* **148**, 433–46.